Steel and Composite Structures, *Vol. 23, No. 2 (2017) 173-186*
DOI: https://doi.org/10.12989/scs.2017.23.2.173

Conceptual configuration and seismic performance of high-rise steel braced frame

Shengfang Qiao [1a], Xiaolei Han [*1], Kemin Zhou [2] and Weichen Li [1]

[1] *School of Civil Engineering and Transportation, South China University of Technology, Tianhe, Guangzhou, 510641, China*
[2] *College of Civil Engineering, Huaqiao University, Jimei, Xiamen, 361021, China*

(*Received September 18, 2016, Revised November 27, 2016, Accepted December 16, 2016*)

Abstract. Conceptual configuration and seismic performance of high-rise steel frame-brace structure are studied. First, the topology optimization problem of minimum volume based on truss-like material model under earthquake action is presented, which is solved by full-stress method. Further, conceptual configurations of 20-storey and 40-storey steel frame-brace structure are formed. Next, the 40-storeystructure model is developed in Opensees. Two common configurations are utilized for comparison. Last, seismic performance of 40-storey structure is derived using nonlinear static analysis and nonlinear dynamic analysis. Results indicate that structural lateral stiffness and maximum roof displacement can be improved using brace. Meanwhile seismic damage can also be decreased. Moreover, frame-brace structure using topology optimization is most favorable to enhance lateral stiffness and mitigate seismic damage. Thus, topology optimization is an available way to form initial conceptual configuration in high-rise steel frame-brace structure.

Keywords: brace; topology optimization; seismic performance; incremental dynamic analysis; high-rise steel frame; pushover

1. Introduction

Steel brace is an available tool to enhance structural lateral stiffness, which was employed to resist wind or strong earthquake in steel frame and also adopted in AISC341-10 (2010). An optimal design method was introduced for steel frame with eccentrically brace by Gong *et al*. (2013). Mojtaba and Massood (2013) studied seismic performance of steel chevron-braced structures using incremental dynamic analysis (or IDA, for short). Shen *et al*. (2015) discussed mechanisms in multi-story frames with X brace (or XB, for short). Tirca *et al*. (2015) used fragility curves to assess seismic resilience of existing braced frame. Seismic performance of different brace configurations are compared using static pushover analysis by Patil and Sangle (2015). Zhang *et al*. (2015) discussed the performance of flexural-shear bracing system in multi-storey steel frame. Steel frames with suspended-zipper brace and inverted v-brace are studied and compared by Ozcelik *et al*. (2016). Some lateral configurations were discussed and applied in braced steel frame, however, few attention was paid to the reasonable lateral brace configurations.

Fortunately, structural configurations in conceptual phase can be formed using structural topology optimization. The configuration of outrigger system was established based on topology optimization by Lee and Tovar (2014). Braced configuration was also emphasized. Liang *et al*. (2000) derived initial lateral braced configuration using topology optimization. Stromberg *et al*. (2012) obtained intial brace configuration with beam/column elements considered. Tangaramvong and Tin-Loi (2015) studied optimized placement of brace for retrofitting steel frames. Rahami *et al*. (2015) used genetic algorithms to study the size and geometry optimization in braced frame. The reasonable distribution of steel brace is studied using optimization method by Aydin *et al*. (2015). Lee *et al*. (2015) discussed the configuration of outrigger truss by topology optimization. Most lateral brace configurations mentioned above are derived by deleting elements or restraining intermediate density, where numerical instability is existing and most optimized configurations are toothed or fuzzy.

In order to solve the problems of numerical instabilities and fuzzy optimized results, the truss-like material model is proposed in Zhou and Li (2005). The braced configuration has been discussed in median and low-rise frame when the natural frequency is constrained in Zhou and Chen (2014). However, load pattern was not considered. The first mode of vibration is dominant in median and low-rise frame, therefore, the braced configuration is discussed with stress constrains under single inverted triangular load pattern in Qiao *et al*. (2016). Nonetheless, the high order modes cannot be neglected in high-rise and ultra high-rise building. Furthermore, the earthquake action is foremost in median and low-rise building, whereas the other load like wind may be more remarkable than earthquake action in high-rise and ultra high-rise building. Hence multiple load patterns need to be considered.

The truss-like material model under multiple load

*Corresponding author, Professor,
E-mail: xlhan@scut.edu.cn
[a] Ph.D. Student, E-mail: sfqiao@yahoo.com

Copyright © 2017 Techno-Press, Ltd.
http://www.techno-press.org/?journal=scs&subpage=6 ISSN: 1229-9367 (Print), 1598-6233 (Online)

patterns is employed in this paper, which can be used to consider multiple load cases and high order modes. Furthermore, the conceptual configurations of high-rise and ultra high-rise steel frame-brace structure are studied using topology optimization (or TPB, for short). In addition, the seismic performance of high-rise braced frame using TPB is studied in OpenSEES (2013).

2. Topology optimization using truss-like material model

2.1 The stiffness matrix

The initial domain in Fig. 1(a) is divided by finite element mesh and full of truss-like material. The truss-like members at any node of elements are presented while members inside the elements are not showed which are demonstrated in Fig. 1(b). Meanwhile truss-like members inside elements can be derived using interpolation theory in Fig. 1(b). The densities and directions of two orthogonal members at any node "j" can be expressed as t_{1j}, t_{2j} and α_j, $\alpha_j + \pi + 2$ in Fig. 1(c) respectively. Elastic matrix along the direction of member under local coordinate system can be represented as

$$\boldsymbol{D}(t_1, t_2, 0) = E \cdot \mathrm{diag}([t_1 \quad t_2 \quad (t_1 + t_2)/4]) \tag{1}$$

E and diag(.) denote elastic modulus and diagonal matrix respectively. When $t_1 = t_2$, truss-like material model is isotropic. Elastic matrix of local coordinate system can be transformed to elastic matrix of the global coordinate system by the coordinate system transformation matrix $T(\alpha)$.

$$\boldsymbol{D}(t_1,t_2,\alpha) = \boldsymbol{T}^{\mathrm{T}}(\alpha)\boldsymbol{D}(t_1,t_2,0)\boldsymbol{T}(\alpha) \tag{2}$$

To simplify the Eq. (2), the matrix are introduced

$$\boldsymbol{A}_1 = \frac{1}{2}\mathrm{diag}[1 \quad -1 \quad 0], \quad \boldsymbol{A}_2 = \frac{1}{4}\begin{bmatrix} 0 & 0 & 1 \\ 0 & 0 & 1 \\ 1 & 1 & 0 \end{bmatrix}, \quad \boldsymbol{A}_3 = \frac{1}{2}\mathrm{diag}[1 \quad 1 \quad \frac{1}{2}] \tag{3}$$

So the Eq. (2) can be written as

$$\boldsymbol{D}(t_1,t_2,\alpha_j) = E\sum_{b=1}^{2} t_{bj} \sum_{r=1}^{3} s_{br} g_r(\alpha_j)\boldsymbol{A}_r \tag{4}$$

r = 1, 2, 3, b = 1, 2. s_{br} and g_r are the elements of following two matrices respectively

$$\boldsymbol{s} = \begin{bmatrix} 1 & 1 & 1 \\ -1 & -1 & 1 \end{bmatrix}, \quad \boldsymbol{g}(\alpha) = \begin{bmatrix} \cos 2\alpha & \sin 2\alpha & 1 \end{bmatrix}, \tag{5}$$

Further, stiffness matrix of element "e" is obtained based on finite element method.

$$\boldsymbol{k}_e = \int_{V_e} \boldsymbol{B}^{\mathrm{T}}\boldsymbol{D}\boldsymbol{B}\,\mathrm{d}V = \sum_{j \in S_e}\sum_{b} t_{bj} \sum_{r} g_r(\alpha_j)\boldsymbol{H}_{ejr} \tag{6}$$

B expresses geometric matrix of element and $\boldsymbol{H}_{ejr} = E\int_{V_e} N_j \boldsymbol{B}^{\mathrm{T}}\boldsymbol{A}_r\boldsymbol{B}\,\mathrm{d}V$ in Eq. (6). Thus, global stiffness matrix can be assembled as follows

$$\boldsymbol{K} = \sum_{e}\boldsymbol{k}_e \tag{7}$$

The truss-like material model was also presented similarly in Qiao and Zhou (2016).

2.2 Optimizedanalysis under single lateral load pattern

In order to consider different lateral load pattern, truss-like model under multiple load cases is employed. Furthermore, the optimized analysis under multiple load cases is based on the optimized analysis under single lateral load pattern in this paper. Therefore, finite element equation is used under single lateral load pattern "l".

$$\boldsymbol{K}\boldsymbol{U}_l = \boldsymbol{F}_l \tag{8}$$

U_l and F_l denote displacement and force vectors under load case l. l = 1, 2,..., L and L is the total number of load cases. Hence strain matrix of single load case "l" can be derived by solving Eq. (8).

$$\boldsymbol{\varepsilon}_l = \boldsymbol{B}\boldsymbol{U}_l = \boldsymbol{B}_l\boldsymbol{K}^{-1}\boldsymbol{F}_l \tag{9}$$

Furthermore, stress matrix in element "e" under single load case l is also be derived.

$$\boldsymbol{\sigma}_{el} = \boldsymbol{D}\boldsymbol{B}\boldsymbol{U}_{el} \tag{10}$$

U_{el} denotes the displacement vectors of element "e". $\boldsymbol{\sigma}_{jl} = [\sigma_{xjl} \quad \sigma_{yjl} \quad \tau_{xyjl}]$ is stress matrix of node "j" in Eq. (10). Thus principal stress direction of node "j" under single load case "l" is acquired.

$$\alpha_{jl} = \frac{1}{2}\arctan\frac{\tau_{xyjl}}{\sigma_{xjl} - \sigma_{yjl}} \tag{11}$$

Two principal stresses of node "j" can be deduced hereinafter.

$$\sigma_{1jl} = \frac{\sigma_{xjl} + \sigma_{yjl}}{2} + \sqrt{\left(\frac{\sigma_{xjl} - \sigma_{yjl}}{2}\right)^2 + \frac{\tau_{xyjl}^2}{4}}, \quad \sigma_{2jl} = \frac{\sigma_{xjl} + \sigma_{yjl}}{2} - \sqrt{\left(\frac{\sigma_{xjl} - \sigma_{yjl}}{2}\right)^2 + \frac{\tau_{xyjl}^2}{4}} \tag{12}$$

Further, two orthogonal truss-like members of node "j" are assigned along two orthogonal principal stress directions like Fig. 1(c), including α_{jl} and $\alpha_{jl} + \pi/2$. The full-stress method is employed herein, which assumes that the stress of truss-like member is the allowable stress. Hence, truss-like member densities of node "j" in any iteration "i" are gained.

$$t_{bjl}^{i+1} = \max(\underline{t}, t_{bjl}^{i}\sigma_{bjl}^{i} / \sigma_p), \quad (b=1,2; j=1,2\cdots n; l=1,2\cdots L) \tag{13}$$

$\underline{t}$ is 10^{-7}, which is used to avoid stiffness matrix singularity. σ_p represents allowable stress.

2.3 Optimized model under multiple load cases

Optimized model using truss-like material model under multiple load cases is demonstrated herein. Moreover, the process of topology optimization under multiple load cases can be described as flow chart in Fig. 1.

$$\begin{aligned} &\text{find} \quad \alpha_j, t_{bj} \geq \underline{t} \quad b=1,2 \\ &\min \quad \sum_e V_e \quad j=1,2,...,n \\ &\text{s.t.} \quad \sigma_{bj}^{l} \leq \sigma_p \quad l=1,2,...,L \end{aligned} \tag{14}$$

The Eq. (14) can be solved by full-stress method under multiple load cases. V_e denotes the volume of truss-like material in element "e". First, two optimal orthogonal principal stress directions α_{jl}, $\alpha_{jl} + \pi/2$ and related densities t_{1jl}, t_{2jl} in Fig. 1(c) can be derived using optimized analysis under every single lateral load pattern "l" in Section 2.2. Thus the L pairs of optimal principal stress directions and related densities under single lateral load can be represented in Fig. 1(d), which are not identical. Meanwhile elastic matrix $D(t_{1jl}, t_{2jl}, \alpha_{jl})$ under every single lateral load is derived. Then the similar ellipse in Fig. 1(d) can be fitted based on the L pairs of optimal principal stress directions and related densities under single lateral load pattern. α_j, $\alpha_j + \pi/2$ and t_{1j}, t_{2j} denote the most unfavorable principal stress directions and related densities under multiple load cases. Moreover, it is assumed the maximum stress of truss-like material under every load case not surpass the allowable stress σ_p. In other words, the stiffness of every optimum structure under single load case should not exceed the stiffness under multiple load cases. Therefore

$$\boldsymbol{D}(\theta; t_{1j}, t_{2j}, \alpha_j) \geq \boldsymbol{D}(\theta; t_{1jl}, t_{2jl}, \alpha_{jl}) \tag{15}$$

Where, the elastic matrix $D(\theta, t_{1j}, t_{2j}, \alpha_j)$, $D(\theta, t_{1jl}, t_{2jl}, \alpha_{jl})$ at any direction θ of node "j" can be obtained as

$$\boldsymbol{D}(\theta; t_{1j}, t_{2j}, \alpha_j) = \boldsymbol{T}(\theta - \alpha_j)^{\mathrm{T}} \boldsymbol{D}(t_{1_j}, t_{2_j}, \alpha_j) \boldsymbol{T}(\theta - \alpha_j) \tag{16}$$

$$\boldsymbol{D}(\theta; t_{1jl}, t_{2jl}, \alpha_{jl}) = \boldsymbol{T}(\theta - \alpha_{jl})^{\mathrm{T}} \boldsymbol{D}(t_{1jl}, t_{2jl}, \alpha_{jl}) \boldsymbol{T}(\theta - \alpha_{jl}) \tag{17}$$

Giventhe correlative elements of matrix $\boldsymbol{D}$, all the elements of matrix $\boldsymbol{D}$ cannot be satisfied in Eq. (15) synchronously according to Zhou and Li (2005). Therefore, the main components D_{11} of matrix $\boldsymbol{D}$ is used to represented the Eq. (15).

$$D_{11}(\theta; t_{1j}, t_{2j}, \alpha_j) \geq \max_l D_{11}(\theta; t_{1jl}, t_{2jl}, \alpha_{jl}) \tag{18}$$

In order to minimize material volume

$$D_{11}(\theta; t_{1j}, t_{2j}, \alpha_j) \approx \max_l D_{11}(\theta; t_{1jl}, t_{2jl}, \alpha_{jl}) \tag{19}$$

The maximum D_{11} under all single load cases is expressed as $S_m(\theta)$

$$S_m(\theta) = \max_l D_{11}(\theta; t_{1jl}, t_{2jl}, \alpha_{jl}) \tag{20}$$

$D_{11}(\theta;\ t_{1j},\ t_{2j},\ \alpha_j)$ can be fitted using $S_m(\theta)$. δ^2 is introduced here.

$$\delta^2 = \left\| S_m(\theta) - D_{11}\left(\theta; t_{1j}, t_{2j}, \alpha_j\right) \right\|_2^2 \tag{21}$$

For simplification, minimizing δ^2 can be used in Zhou and Li (2005). Since the θ is continuous

$$\begin{aligned} \delta^2 &= \int \left[S_m(\theta) - D_{11}\left(\theta; t_{1j}, t_{2j}, \alpha_j\right) \right]^2 \mathrm{d}\theta \\ &= \int_0^{\pi} D_{11}\left(\theta; t_{1j}, t_{2j}, \alpha_j\right)^2 \mathrm{d}\theta - 2\int_0^{\pi} D_{11}\left(\theta; t_{1j}, t_{2j}, \alpha_j\right) \cdot \\ &\cdot S_m(\theta) \mathrm{d}\theta + \int_0^{\pi} S_m(\theta)^2 \mathrm{d}\theta \end{aligned} \tag{22}$$

The Eq. (22) can be adapted

$$\delta^2 = \delta_1^2 + \left\| S_m(\theta) \right\|_2^2 \tag{23}$$

Where, $\|S_m(\theta)\|_2^2$ is not related to t_{1j}, t_{2j}, α_j.

$$\begin{aligned} \delta_1^2 &= \frac{\pi E^2}{8} [2(t_{1j} + t_{2j})^2 + (t_{1j} - t_{2j})^2] - \\ &\pi E^2 [(t_{1j} + t_{2j}) I_0 + (t_{1j} - t_{2j})(I_1 \cos 2\alpha_j + I_2 \sin 2\alpha_j)] \end{aligned} \tag{24}$$

I_0, I_1 and I_2 can be calculated

$$I_{[0,1,2]} = \frac{1}{\pi E} \int_0^{\pi} S_m(\theta) [1, \cos 2\theta, \sin 2\theta] \mathrm{d}\theta \tag{25}$$

The derivative formulas can be derived from Eq. (24).

$$\begin{aligned} \frac{8}{\pi E^2} \frac{\partial \delta_1^2}{\partial t_{1j}} &= 4\left(t_{1j} + t_{2j}\right) + 2\left(t_{1j} - t_{2j}\right) \\ &- 8[I_0 + (I_1 \cos 2\alpha_j + I_2 \sin 2\alpha_j)] = 0 \end{aligned} \tag{26}$$

$$\begin{aligned} \frac{8}{\pi E^2} \frac{\partial \delta_1^2}{\partial t_{2j}} &= 4\left(t_{1j} + t_{2j}\right) - 2\left(t_{1j} - t_{2j}\right) \\ &- 8[I_0 - (I_1 \cos 2\alpha_j + I_2 \sin 2\alpha_j)] = 0 \end{aligned} \tag{27}$$

$$\frac{8}{\pi E^2} \frac{\partial \delta_1^2}{\partial \alpha_j} = -16(t_{1j} - t_{2j})\left(-I_1 \sin 2\alpha_j + I_2 \cos 2\alpha_j\right) = 0 \tag{28}$$

Thus the α_j can be solved in Eq. (28). Then t_{1j}, t_{2j} can also be derived from Eqs. (26)- (27).

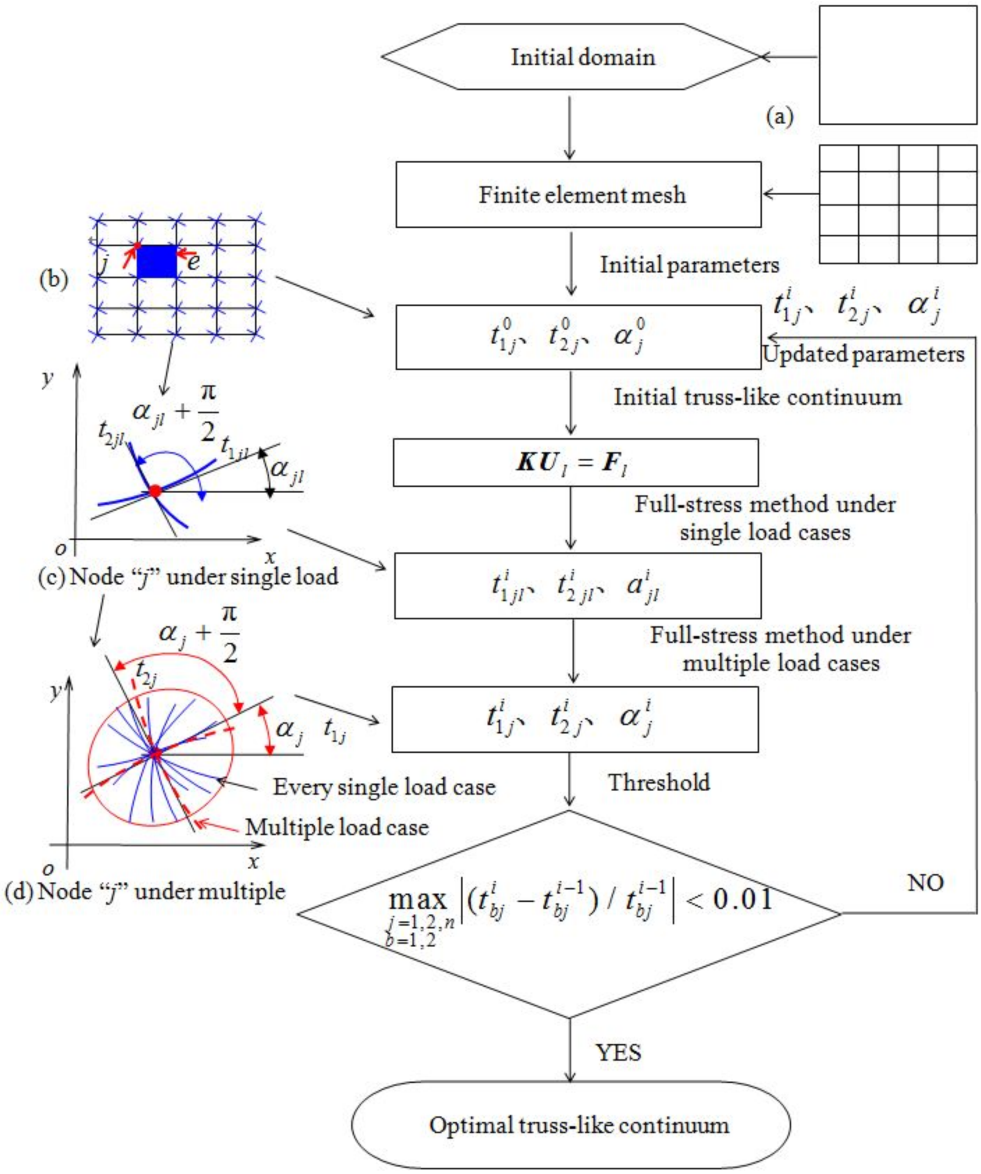

Fig. 1 Optimized model under multiple load cases

The convergence condition is presented as follows

$$\delta = \max_{\substack{j=1,2,n\\b=1,2}} \left| \frac{t_{bj}^{i+1} - t_{bj}^{i}}{t_{bj}^{i}} \right|$$

If $\delta \leq 1\%$, this analysis is finished. Since truss-like member densities inside elements can be derived using interpolation theory, optimized truss-like continuum is gained.

3. Numerical cases

3.1 High-rise steel frame

2D 20-storey steel frame is demonstrated in Fig. 2(a). I–shape section information of 20-storey steel frameis also presented in Fig. 2(a). Similarly, original 40-storey steel frame (or OF, for short) is displayed in Fig. 2(b). I section information for columns and beams are demonstrated in Tables 1 and 2 respectively. Moreover, concentrated mass is 16.0 ton in every beam-column connection. Uniform distributed load is 25.0 KN/m (including dead and live load) on beams. The site predominant period is 0.35 s and seismic peak ground acceleration is 0.22 g in GB50011 (2010). The corresponding probability of exceedance is 2% in 50 years.

3.2 Optimized brace configuration

First, FEM mesh of initial design domain is divided by 640 rectangular elements as shown in Fig. 3(a). Then every nodeinany rectangular element is enhanced by two truss-like members. In addition, members inside every element are calculated based on interpolation method and not presented in Fig. 3(b). Thus initial truss-like continuum is formed. Elastic Modulus E is 206 Gpa and allowable stress of truss-like material is 235 Mpa.

Next, total seismic action F is assumed as 1.2% of total weight G in GB50011 (2010).

Table 1 Member section for 20-storey frame (mm)

Columns for 1-10 storey*	Columns for 11-20 storey	Beams for 1-20 storey
400×400×12×14	300×400×10×12	200×400×10×12

*width×height×flange thickness×web thickness of I section for 1-10 storey column

Table 2 Member section for 40-storey frame (mm)

Columns for 1-10 storey	Columns for 11-20 storey	Beams for 1-40 storey
500×500×16×14	450×450×12×14	200×400×10×12
Columns for 21-30 storey	Columns for 31-40 storey	
400×400×12×14	300×400×10×12	

$$F = 0.012G = 0.012\sum_{i=1}^{n} G_i \tag{29}$$

Several lateral seismic load patterns can be determined based on FEMA-356 (2000) as follows.

Proportional height lateral seismic load pattern: Case 1

$$F_i = \frac{G_i h_i^k}{\sum_{j=1}^{n} G_j h_j^k} F \tag{30}$$

Where, G_i and F_i represent seismic action and floor weight of storey i. h_i denotes height from the base to storey i. k = 2.0 when $T \geq 2.5$ s, whereas k = 1.0 when $T \leq 0.5$ s. The high modes can be considered in this load pattern.

Elastic first mode lateral seismic load pattern: Case 2

$$F_i = \frac{\phi_{1i}}{\sum_{j=1}^{n} \phi_{1j}} F \tag{31}$$

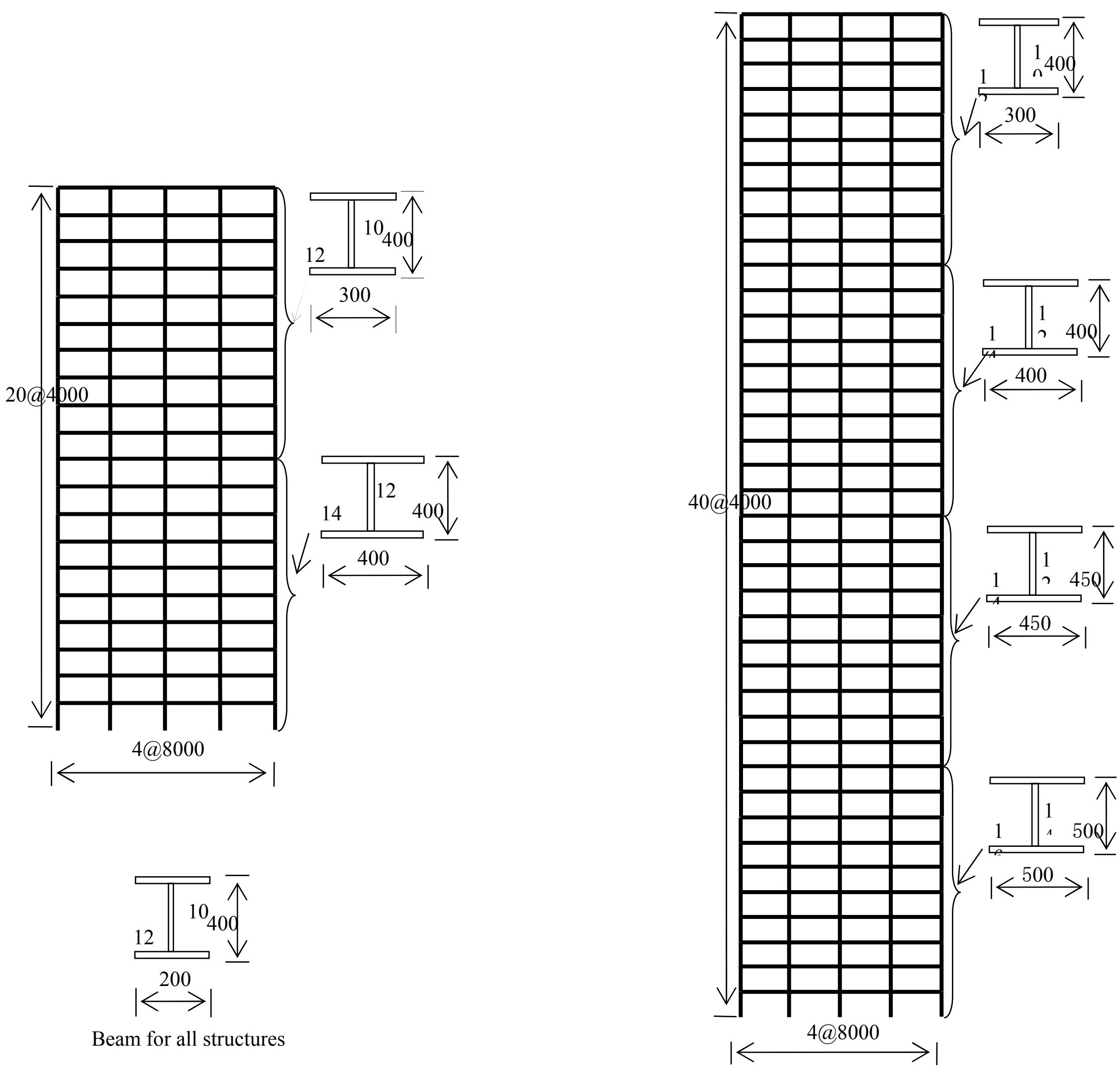

(a) 20-storey steel frame (b) 40-storey steel frame

Fig. 2 Structure diagram (mm)

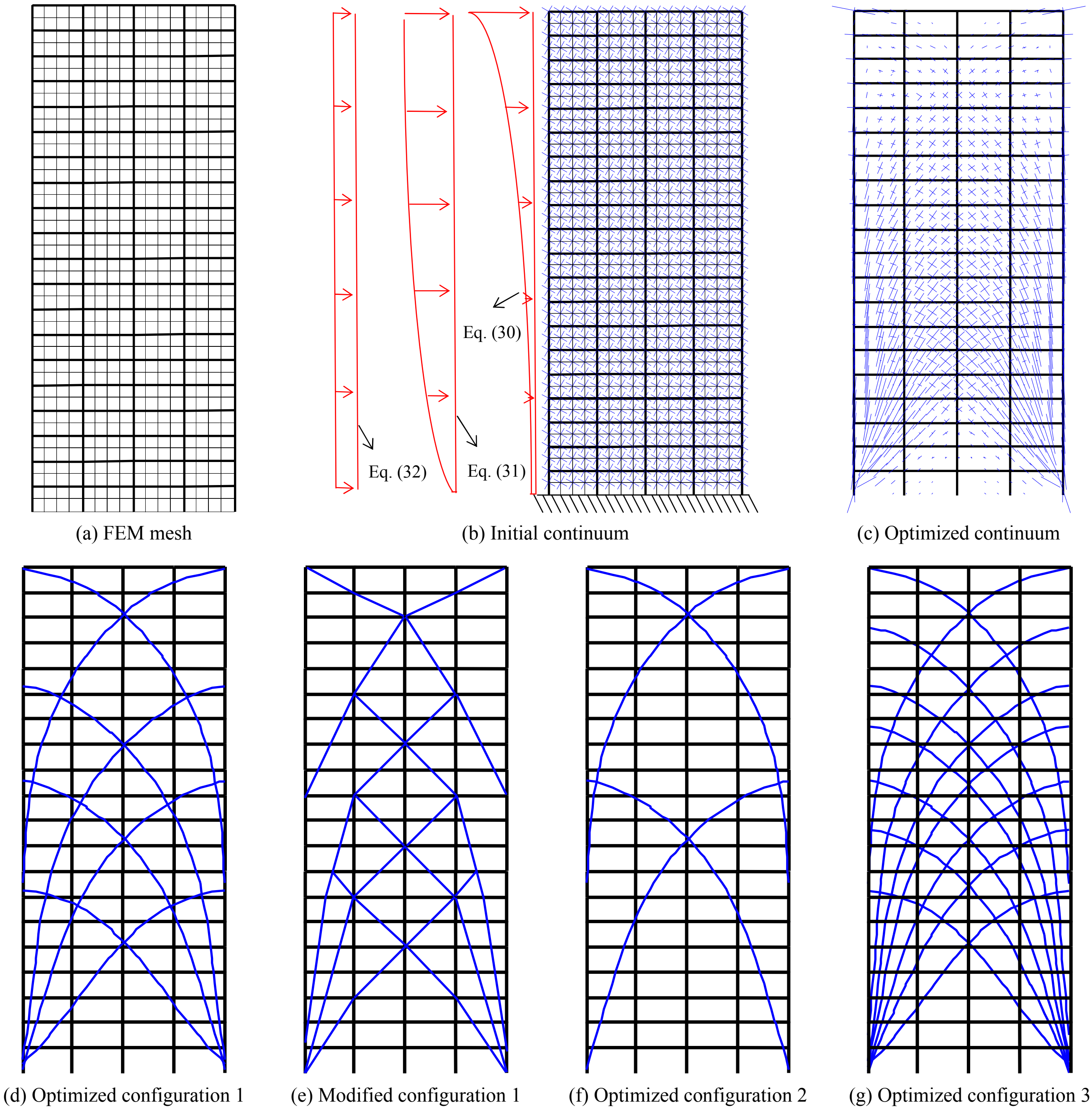

Fig. 3 Optimized analysis of 20-storey frame structure

Where, ϕ_{1i} signifies the first mode displacement.

Proportional mass lateral seismic load pattern: Case 3

$$F_i = \frac{G_i}{\sum_{j=1}^{n} G_j} F \tag{32}$$

The effective mass factor is used

$$\alpha_m = \frac{(\sum_{i=1}^{n} G_i \phi_{mi} / g)^2}{(\sum_{i=1}^{n} G_i / g)(\sum_{i=1}^{n} G_i \phi_{mi}^2 / g)} \tag{33}$$

α_m signifies effective mass factor of vibration mode m. According to Eqs. (30)-(32), several lateral load patterns can be presented in Fig. 3(b). Furthermore, base is fixed completely.

Last, optimized truss-like continuum is established after FEM analysis, which is depicted in Fig. 3(c). Intermediate density is not restrained in the iterative process of truss-like material model, therefore, the numerical instabilities are avoided. The optimized truss-like continuum is difficult to be manufactured directly, because it is formed by numerous truss-like members.

In order to make more conveniently, the optimized discrete configuration is proposed using discrete method in Zhou and Li (2005). The discrete method can be interpreted

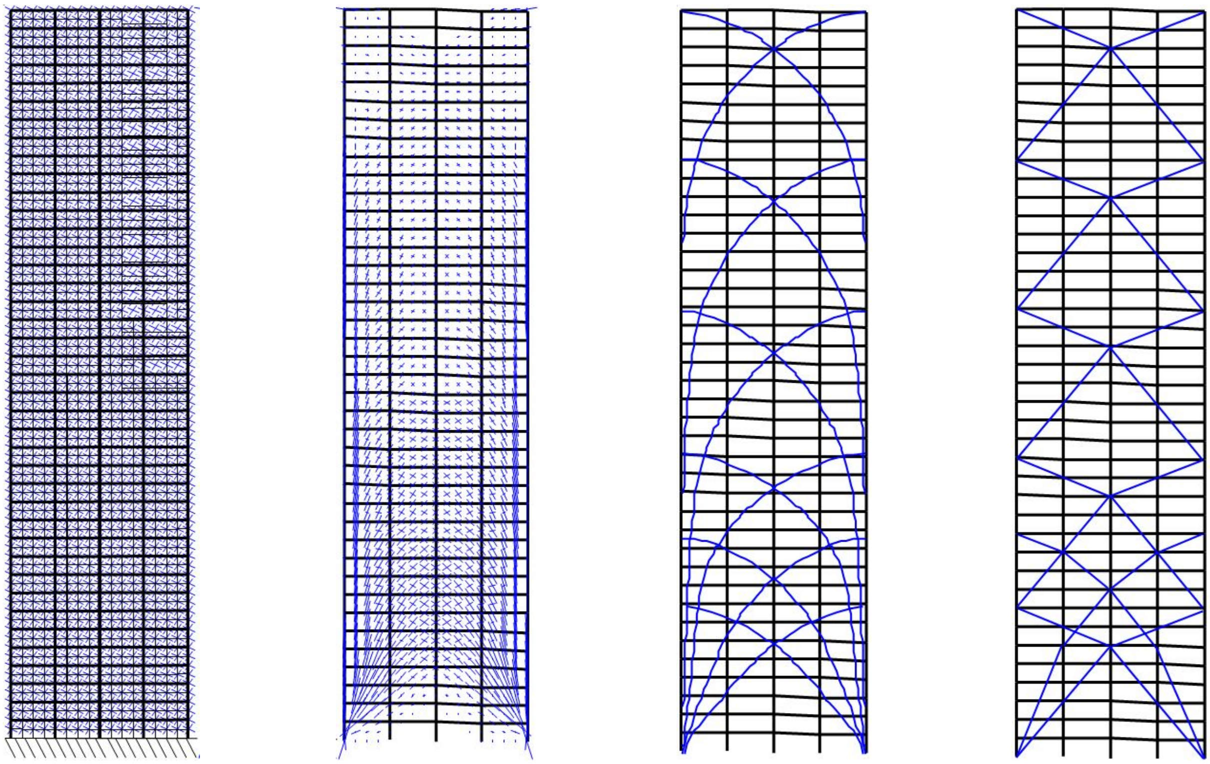

(a) FEM mesh (b) Optimized continuum (c) Optimized configuration (d) Modified configuration

Fig. 4 Optimized analysis of 40-storey frame

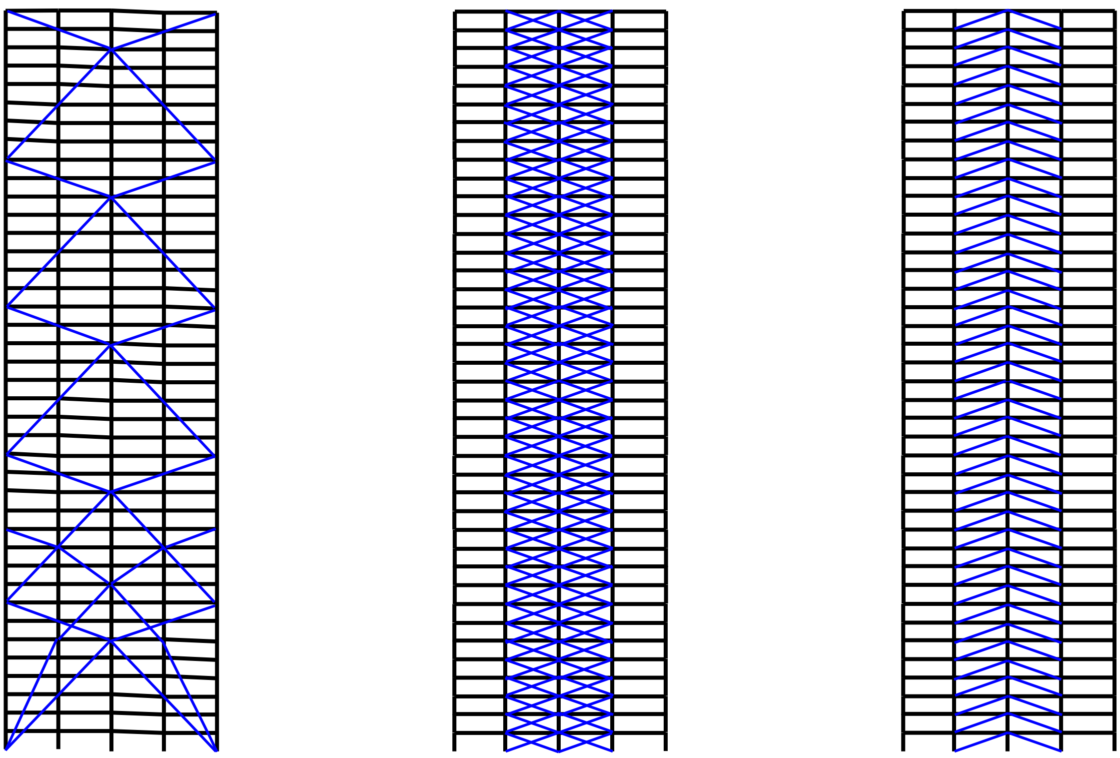

(a) TPB configuration (b) XB configuration (c) SBB configuration

Fig. 5 Bracing system of 40-storey frame structure

as follows. The points need members to be connected based on equilibrium conditions, where point forces act. Given curves of nonvanishing curvature, distributed members are also needed. Therefore, the points acted upon by point forces can be taken as the starting points of continuum curves. Similarly, other starting points can be determined

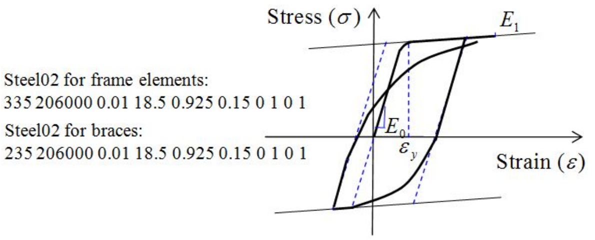

Fig. 6 Constitutive relation of steel

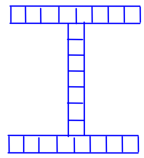

Fig. 7 Fiber section

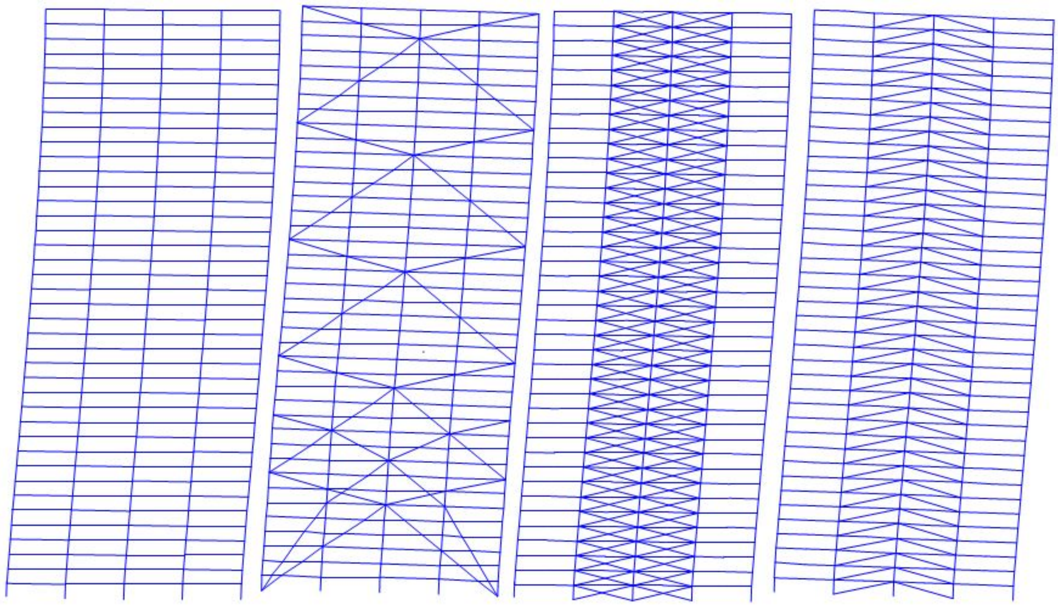

(a) OF (b) TPB (c) XB (d) SBB

Fig. 8 First modes

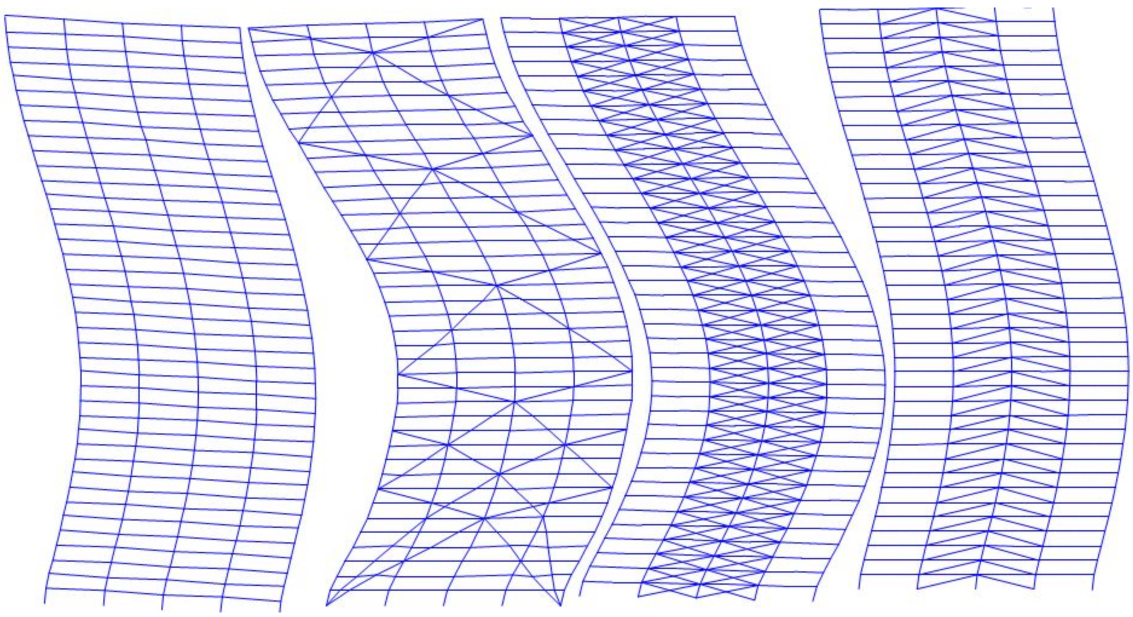

(a) OF (b) TPB (c) XB (d) SBB

Fig. 9 Second modes

along the curve. Finally, the optimized discrete configuration can be established in Fig. 3(d). Moreover, modified configuration is derived by merging nearby nodes in Fig. 3(e) for fabricating more easily. Different discrete configura-

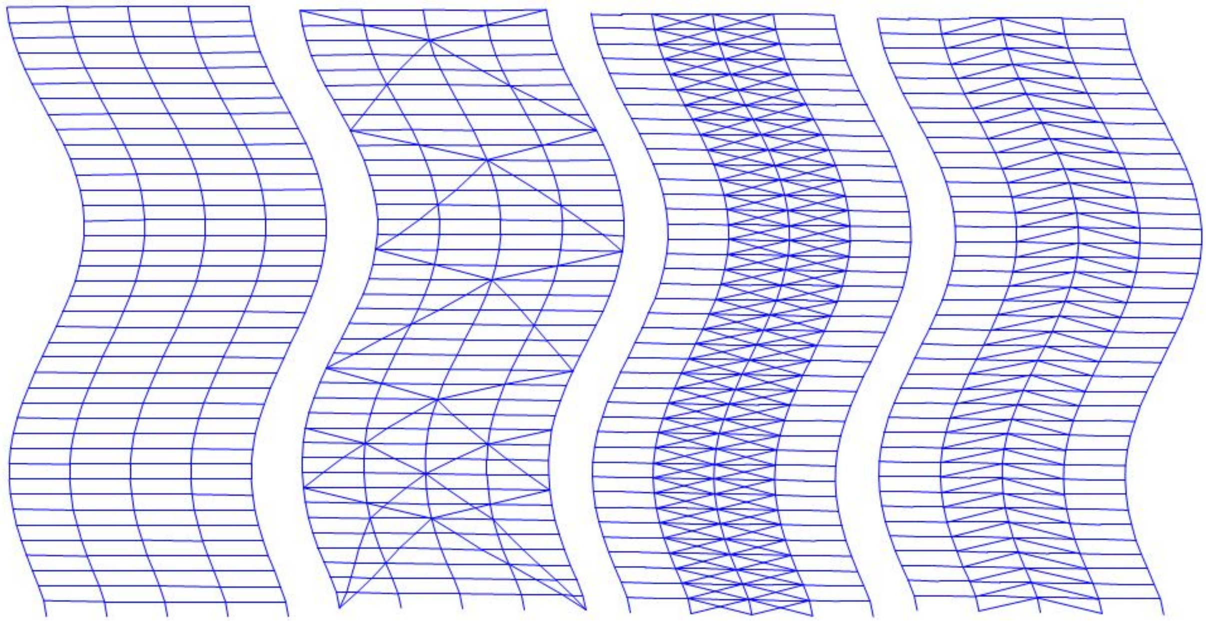

(a) OF (b) TPB (c) XB (d) SBB

Fig. 10 Third modes

Table 3 Braces of 40-storey frame

Brace configuration	TPB	XB	SBB
Sectional area (mm^2)	365	150	300
Total length (m)	587.2	1430.4	715.2
Total volume (m^3)	0.214	0.214	0.214
Element	Truss	Truss	Truss
Material constitutive	Steel02	Steel02	Steel02
Yield stress (MPa)	235	235	235
Elastic modulus (MPa)	206000	206000	206000

Table 4 The first three periods

Configuration	T1	T2	T3
OF (s)	12.37	4.16	2.40
Accumulated mass factor	0.774	0.884	0.920
TPB (s)	9.25	3.13	1.82
Accumulated mass factor	0.751	0.889	0.929
XB (s)	9.76	3.24	1.83
Accumulated mass factor	0.771	0.890	0.927
SBB (s)	9.78	3.25	1.84
Accumulated mass factor	0.771	0.890	0.926

tions can also be formed in Figs. 3(f)-(g). Of course reasonable brace configuration should be established according to actual engineering requirement.

Likewise, the 40-storey optimized truss-like continuum can be obtained in Fig. 4(b). In addition, the discrete configuration in Fig. 4(c) is derived using discrete method. The modified brace configuration of 40-storey steel frame is also presented in Fig. 4(d).

Table 5 Comparison

OF	T1	T2	T3
OpenSEES (s)	12.37	4.16	2.40
Accumulated mass factor	0.774	0.884	0.920
Perform-3d (s)	12.43	4.18	2.41
Accumulated mass factor	0.774	0.884	0.919
Error of periods (%)	0.48	0.48	0.41

3.3 Modelin OpenSEES

Lateral brace configuration of topology optimization (or TPB, for short) for 40-storey steel frame in Fig. 4(c) is used in Fig. 5(a). Furthermore, X-brace (or XB, for short) and Single-bar brace (or SBB, for short) are utilized for comparison, which are presented in Figs. 5(b)-(c) respectively.

Sections of beams and columns are introduced in Fig. 2(b). Steel02 in Opensees (2013) is employed to represent material constitutive of steel in Fig. 6 which yielding stress is 335 Mpa and hardening parameter is 0.01. Moreover, elements for beam and column are simulated using nonlinear Beam Column with fiber section in Fig. 7 Second-order (P-Δ) effects is taken into account for column element. Similarly, detailed information of brace is tabulated in Table 3 respectively. Furthermore, total volumes of different brace are same in Table 3.

The first three periods and relevant effective mass factor of OF (short for original frame), TPB, XB and SBB are derived in Table 4 using Opensees (2013). The first three modes of vibration are also demonstrated in Figs. 8-10 correspondingly. Additionally, the OF is simulated in software Perform-3d and FEMA Beam/ Column with lumped plastic hinges are utilized for beams/columns. The

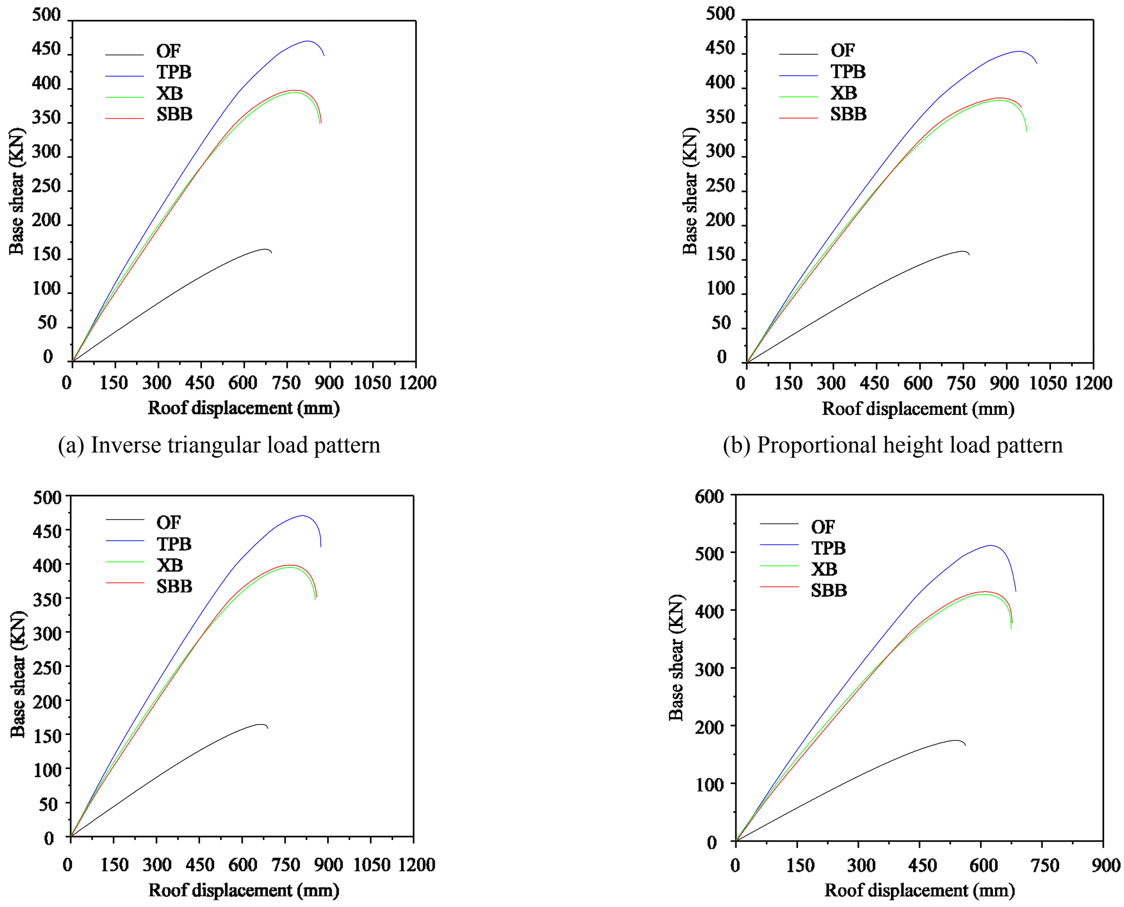

(a) Inverse triangular load pattern

(b) Proportional height load pattern

(c) First modal load pattern

(d) Uniform load pattern

Fig. 11 Pushover curves of different load mode

first three periods of OF are established for comparison in Table 5. The accumulated mass factor is also solved using Eq. (33) and presented in Table 5.

3.4 Static nonlinear analysis

Static nonlinear analysis (Pushover) under different lateral load pattern is carried out in Opensees (2013). Proportional height lateral load pattern is inverse triangular load pattern when k = 1.0 in Eq. (30). The corresponding pushover curves of OF, TPB, XB and SBB can be depicted in Fig. 11(a). Similarly, the pushover curves can be derived in Fig. 11(b) when k = 2.0. The curves using load pattern based on Eqs. (31) and (32) are also demonstrated in Fig. 11(c) and in Fig. 11(d).

3.5 Time history analysis

In order to assess the seismic vulnerability of structures, a series of nonlinear time-history analyses for 40-storey structures are conducted in OpenSEES (2013). 22 far field earthquake records (E1~E22) in Table 6 are used from FEMA P-695 (2009). The first and second modes of structures were assigned a Rayleigh damping with 5%. IDA is employed in Vamvatsikos and Cornell (2002). Maximum inter story drift ratio of each time-history analysis is plotted as a point in Fig. 12. Thus, a suite of points are presented in Figs. 12(a)-(d) under different peak ground accelerations (or PGA, for short).

Storey drift limits of Immediate Occupancy (or IO, for short), Moderate Damage (or SD, for short) and Severe Damage (or SD, for short) are derived in Table 7 based on GB50011 (2010). The state of dynamic instability in Vamvatsikos and Cornell (2002) or maximum interstory drift ratio over 10% in FEMA273 (1997) is regarded as collapse prevention (or CP, for short). Furthermore, cumulative probability curves of IO, MD, SD and CPare derived in Figs. 12(a), (c), (e) and (g). The logarithmic curves fitting can also beestablished in Figs. 12(b), (d), (f) and (h) correspondingly.

4. Discussion

The brace configurations using topology optimization of 20- storey and 40- storey high-rise frames were presented in Figs. 3 and 4. The results manifest that numerical instabilities are settled, including unshaped optimized configuration and checkerboard phenomenon. Furthermore, more details for further design and different configurations can also be presented based on truss-like model than Liang *et al.* (2000).

The first periods of TPB, XB and SBB decrease 25.1%, 21.1% and 20.9% than OF respectively in Table 4. It can be

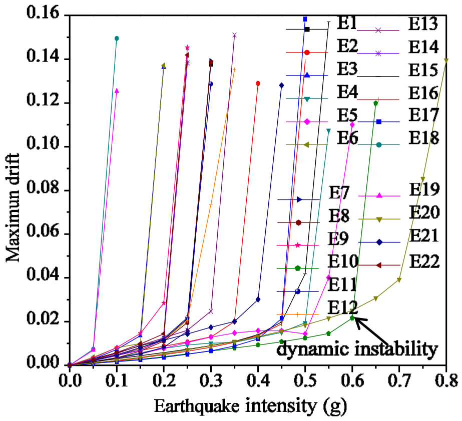

(a) IDA curves of OF

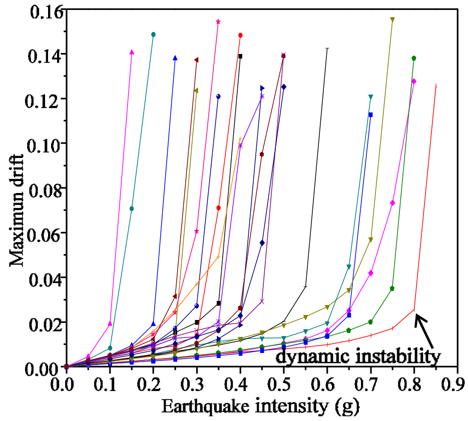

(b) IDA curves of TPB

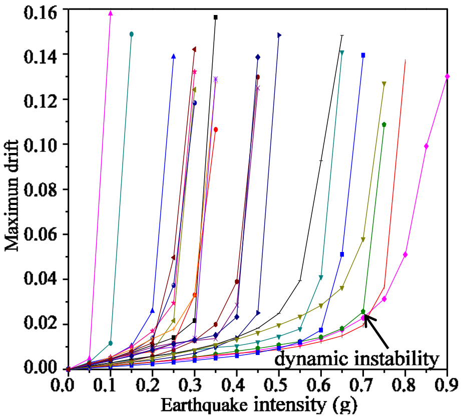

(c) IDA curves of XB

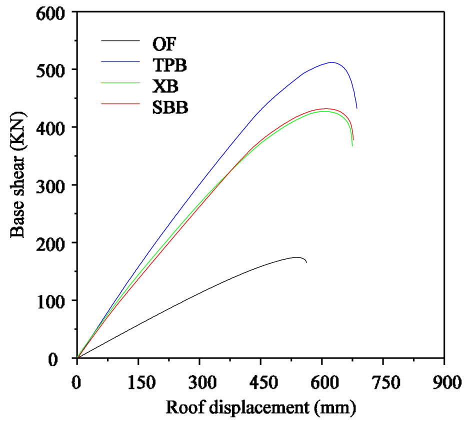

(d) IDA curves of SBB

Fig. 12 IDA curves of 40-storey frame

Table 6 Earthquake records

Event	Year	Abbreviation	Duration(s)
San_Fernando	1971	E1	20
San_Fernando	1971	E2	20
Friuli-Italy-01	1976	E3	20
Imperial_Valley-06	1979	E4	20
Imperial_Valley-06	1979	E5	20
Superstition_Hills-02	1987	E6	20
Superstition_Hills-02	1987	E7	20
Loma_Prieta	1989	E8	20
Loma_Prieta	1989	E9	20
Cape_Mendocino	1992	E10	20
Landers	1992	E11	20
Landers	1992	E12	20

Table 6 Continued

Event	Year	Abbreviation	Duration(s)
Northridge-01	1994	E13	20
Northridge-01	1994	E14	20
Kobe-Japan	1995	E15	20
Kobe-Japan	1995	E16	20
Kocaeli-Turkey	1999	E17	20
Kocaeli-Turkey	1999	E18	20
Chi-Chi-Taiwan	1999	E19	20
Chi-Chi-Taiwan	1999	E20	20
Duzce-Turkey	1999	E21	20
Hector_Mine	1999	E22	20
Northridge-01	1994	E13	20
Northridge-01	1994	E14	20

gleaned from that the initial lateral stiffness improves because of adding braces to the structures. The second and third periods also point toward the same trend in Table 4. Furthermore, the structure using TPB is most effective to increase lateral stiffness and the XB is similar to SBB.

The pushover curves represent global response of the structures under different lateral load pattern in Figs. 11(a)-(d). The maximum base shear V_{max} and roof displacement u_{max} of different structures under the different lateral load patterns are derived in Table 7. In case of inverse triangular load pattern, the maximum base shears of TPB, XB and SBB enhance 185.36%, 139.53% and 141.60%. Moreover, the corresponding maximum roof displacements augment 26.46%, 24.23% and 25.03% severally. The similar trend can also be indicated in others lateral load patterns. It can be inferred the high-rise structures with braces fortify both

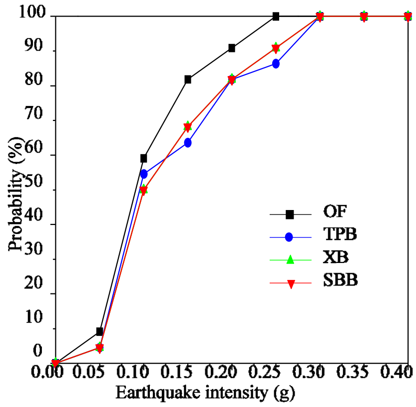

(a) Cumulative probability of IO

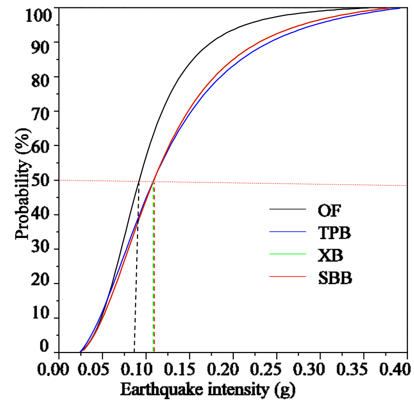

(b) Logarithmic curve fitting of IO

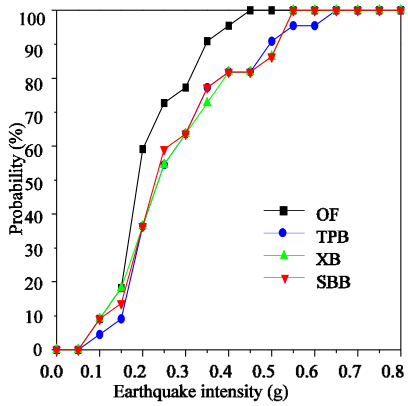

(c) Cumulative probability of MD

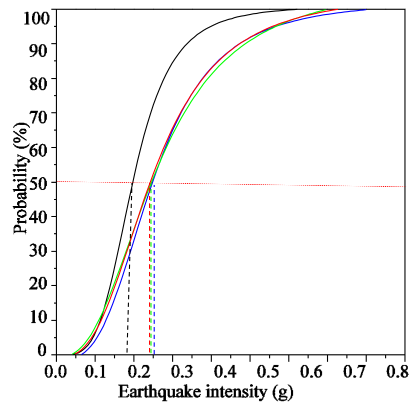

(d) Logarithmic curve fitting of MD

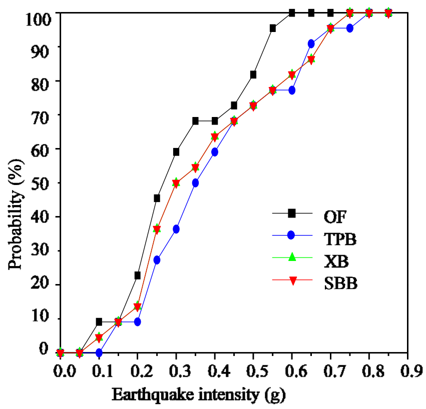

(e) Cumulative probability of SD

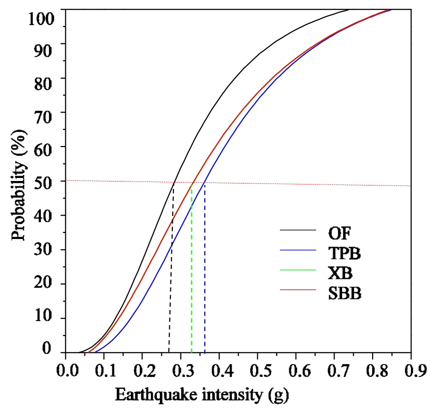

(f) Logarithmic curve fitting of SD

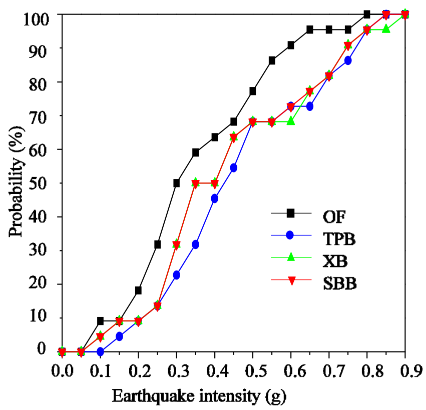

(g) Cumulative probability of CP

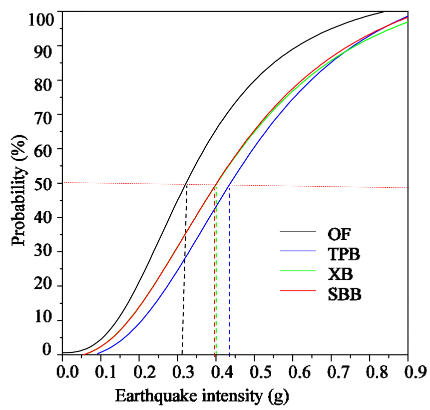

(h) Logarithmic curve fitting of CP

Fig. 13 Curves of cumulative probability under different performance state

Table 7 Maximum base shear and roof displacement

(a) Inverse triangular

Inverse triangular	V_{max} (KN)	u_{max} (mm)
OF	164.72	695.04
TPB	470.04	878.97
XB	394.56	863.45
SBB	397.97	869.01

(b) Proportional height

Proportional height	V_{max} (KN)	u_{max} (mm)
OF	162.5	770.04
TPB	454.03	1003.97
XB	382.42	968.45
SBB	386.01	977.01

(c) First modal

First modal	V_{max} (KN)	u_{max} (mm)
OF	164.66	690.04
TPB	470.74	875.97
XB	394.83	855.45
SBB	398.19	861.01

(d) Uniform load

Uniform load	V_{max} (KN)	u_{max} (mm)
OF	174.22	562.04
TPB	511.91	685.97
XB	427.04	674.45
SBB	431.69	677.01

Table 8 Median capacity

State	OF	TPB	XB	SBB
IO(g)	0.091	0.109	0.109	0.109
MD(g)	0.196	0.251	0.246	0.242
SD(g)	0.286	0.365	0.337	0.337
CP(g)	0.322	0.441	0.405	0.404
CMR	1.46	2.01	1.84	1.84

maximum base shear and maximum roof displacement. Additionally, TPB is most advisable.

The cumulative probability curves of structures under different performance state were depicted in Fig. 13. Median capacity of cumulative probability under performance state of IO is calculated in Table 8. It denotes the same increasing value of median capacity for different brace configurations under IO state. Similarly, median capacity of MD, SD and CP state are established in Table 8. Moreover, the collapse margin ration (or CMR, for short) in FEMA P-695 (2009) is derived in Table 8. However, median capacity of TPB, XB and SBB enhance 28.1%, 25.5% and 23.5% than OF under MD state. Further, the similar tendency under SD and CP state can be demonstrated in Table 8. It can be concluded the frame-brace structures can reduce seismic vulnerability than pure frame. The CMR of TPB, XB and SBB is also improved 37.7%, 26.0% and 26.0% respectively. In addition, TPB is most favorable to mitigate different damage states and the XB is close to SBB.

5. Conclusions

Conceptual configuration and seismic analysis of high-rise steel frame-brace structure are discussed. Brace configuration is formed using topology optimization. Further, seismic performance of different configurations are studied and compared. Several following conclusions could be drawn based on the results of this study.

- Topology optimization is an available tool to form braced configuration in high-rise and ultra high-rise steel frame. Conceptual configuration based on truss-like model can depict more details for designing and constructing. Different braced configuration can be also derived, therefore, more engineering requirement can be satisfied. Further, numerical instability is resolved.
- The lateral stiffness and maximum roof displacement can be improved using braces. Moreover, the frame-brace structure with TPB is most acceptable than XB and SBB. The XB is similar to SBB.
- The seismic damage states can be reduced using braces. In addition, TPB is most favorable to mitigate seismic damage and resist collapse.

Acknowledgments

The research described in this paper was financially supported by the Natural Science Foundation of China (Granted No 51378221, 11572131), the State Key Laboratory of Subtropical Building Science Foundation of SCUT (Granted No 2014ZC16, No 2015ZA05) and Guangzhou science and technology projects (Granted No 15020088).

References

AISC341-10 (2010), Seismic Provision for Structure Steel Buildings; American Institute of Steel Construction, Chicago, IL, USA.

Aydin, E., Sonmez, M. and Karabork, T. (2015), "Optimal placement of elastic steel diagonal braces using artificial bee colony algorithm", *Steel Compos. Struct., Int. J.*, **19**(2), 349-368.

FEMA 273 (1997), NEHRP guidelines for the seismic rehabilitation of buildings; Federal Emergency Management Agency, Washington, USA.

FEMA 356 (2000), Prestandard and commentary for the seismic rehabilitation of buildings; Federal Emergency Management Agency, Washington, USA.

FEMA P695 (2009), Quantification of building seismic performance factors; Federal Emergency Management Agency, Washington, USA.

GB50011 (2010), Code for Seismic Design of Buildings; Architecture Industry Press, Beijing, China.

Gong, Y.L., Xue, Y.S. and Xu, L. (2013), "Optimal capacity design of eccentrically braced steel frameworks using nonlinear

response history analysis", *Eng. Struct.*, **48**, 28-36.
Lee, S. and Tovar, A. (2014), "Outrigger placement in tall buildings using topology optimization", *Eng. Struct.*, **74**(6), 122-129.
Lee, D.k., Shin, S., Lee, J.h. and Lee, K. (2015), "Layout evaluation of building outrigger truss by using material topology optimization", *Steel Compos. Struct., Int. J.*, **19**(2), 263-275
Liang, Q.Q., Xie, Y.M. and Steven, G.P. (2000), "Optimal topology design of bracing systems for multistory steel frames", *J. Struct. Engrg.*, **126**(7), 823-829.
Mojtaba, F. and Massood, M. (2013), "On the quantification of seismic performance factors of Chevron Knee Bracings in steel structures", *Eng. Struct.*, **46**, 155-164.
Ozcelik, Y., Saritas, A. and Clayton, P.M. (2016), "Comparison of chevron and suspended-zipper braced steel frames", *J. Construct. Steel Res.*, **119**(3), 169-175.
Opensees (2013), Open system for earthquake engineering simulation, Pacific Earthquake Engineering Research Center, University of California, Berkeley, CA, USA. http://opensees.-berkeley.edu
Patil, D.M. and Sangle, K.K. (2015), "Seismic behaviour of different bracing systems in high rise 2-D steel buildings", *Structures*, **3**, 282-305.
Qiao, S.F., Han, X.L., Zhou, K.M. and Ji, J. (2016), "Seismic analysis of steel structure with brace configuration using topology optimization", *Steel Compos. Struct., Int. J.*, **21**(3), 501-515.
Qiao, S.F. and Zhou, K.M. (2016), "Structural topology optimization under uncertain load based on truss-like material model", *Eng. Mech.*, **33**(3), 252-256. [In Chinese]
Rahami, H., Kaveh, A. and Shojaei, I. (2015), "Swift analysis for size and geometry optimization of structures", *Adv. Struct. Eng.*, **18**(3), 365-380.
Shen, J., Wen, R. and Akbas, B. (2015), "Mechanisms in two-story X-braced frames", *J. Construct. Steel Res.*, **106**(3), 258-277.
Stromberg, L.L., Beghini, A., Baker, W.F. and Paulino, G.H. (2012), "Topology optimization for braced frames: combining continuum and beam/column elements", *Eng. Struct.*, **37**(2), 106-124.
Tangaramvong, S. and Tin-Loi, F. (2015), "Optimal performance-based rehabilitationof steel frames using braces", *J. Struct. Eng.*, **141**(10), 1-10(04015015).
Tirca, L., Serban, O., Lin, L., Wang, M. and Lin, N. (2015), "Improving the seismic resilience of existing braced-frame office buildings", *J. Struct. Eng.*, **141**(7), 1-14.
Vamvatsikos, D. and Cornell, C. (2002), "Incremental dynamic analysis", *Earthq. Eng. Struct. Dyn.*, **31**(3), 491-514.
Zhang, L., Tong, G.S. and Ji, Y. (2015), "Buckling of flexural-shear bracing system and its braced steel frames", *Adv. Struct. Eng.*, **18**(11), 1831-1844.
Zhou, K.M. and Chen, C.H. (2014), "Topology optimization of frame bracing system for natural frequency", *The Open Civil Eng. J.*, **8**(1), 250-256.
Zhou, K.M. and Li, X. (2005), "Topology optimization of Structures under multiple load cases using a fiber-reinforced composite material model", *Computat. Mech.*, **38**(5), 163-170.

CC